Structure-dependent magnetoresistance and spin-transfer torque in antiferromagnetic Fe|MgO|FeMn|Cu tunnel junctions

Xingtao Jia*
School of Physics and Electronic Information Engineering, Henan Polytechnic University, Jiaozuo 454000, China

Huimin Tang and Shizhuo Wang
Department of Physics, Beijing Normal University, Beijing 100875, China

Minghui Qin
Institute for Advanced Materials and Laboratory of Quantum Engineering and Quantum Materials, South China Normal University, Guangzhou 510006, China

(Received 17 September 2016; revised manuscript received 17 January 2017; published 2 February 2017)

We predict large magnetoresistance (MR) and spin transfer torque (STT) in antiferromagnetic Fe|MgO|FeMn|Cu tunnel junctions based on first-principles scattering theory. MR as large as ∼100% is found in one junction. Magnetic dynamic simulations show that STT acting on the antiferromagnetic order parameter dominates the spin dynamics, and an electronic bias of order 10^{-1} mV and current density of order 10^5 Acm^{-2} can switches a junction of three-layer MgO, they are about one order smaller than that in Fe|MgO|Fe junction with the same barrier thickness, respectively. The multiple scattering in the antiferromagnetic region is considered to be responsible for the enhanced spin torque and smaller switching current density.

DOI: 10.1103/PhysRevB.95.064402

I. INTRODUCTION

Due to high stability to a parasitic magnetic field and high working frequency, antiferromagnet (AFM)-based spintronics [1–3] has attracted much attention both experimentally [4–16] and theoretically [17–29]. Similar to ferromagnet (FM)-based magnetic structures, AFM-based structures also have magnetoresistances (MR) [8–12] to distinguish information states that can be controlled by spin transfer torque (STT) [16–27], photomagnetic pulses [4–7], and spin wave [30]. Relativistic spin-orbit torques provide a new powerful tool to control the magnetization [31–33]. A field-driven AFM domain-wall velocity induced by Néel spin-orbit torques can be two orders of magnitude larger than that of the FM domain wall [34]. Sizable spin torque from enhanced spin Hall effects in a AFM|normal metal (NM)|FM spin valve (SV) has been demonstrated [35,36]. However, the poor size-scalability overshadows the application of the spin-orbit effect [2].

Anisotropic MR (AMR) in AFM-based magnetic structures such as NM|AFM [8–11] and FM|AFM [35,36] contacts is relatively small (∼1%). However, if a MgO barrier is inserted between NM and AMF, a large AMR of up to 100% is observed at low temperatures [12]. Similar to FM-based SVs, a reference (ferromagnetic or antiferromagnetic) polarizer can be introduced to form an antiferromagnetic SV, where a nonrelativistic structure-dependent MR dominates over the relativistic MR [12,17,18]. Indeed, antiferromagnetic SVs, especially perpendicular ones, show merit for large MR, electronic control, and size-scalability.

Recently, an ultralow switching current density below 10^6 Acm^{-2} was predicted in the antiferromagnetic metal-based SVs [17,37], where the spin torque acting on the antiferromagnetic order parameter in the whole AFM region. Generally, switching current density is proportional to Gilbert damping coefficient, but inversely proportional to spin transfer efficiency [17]. Enhanced spin transfer efficiency from multiple reflection was demonstrated in a MgO-based tunnel junctions [38]. Because multiple reflection can exist naturally in the AFM, enhanced spin transfer and lower switching current density are expected in the AFM-based magnetic structures.

Here, we focus on the antiferromagnetic Fe|MgO|FeMn|Cu junctions, for which γ-FeMn is a well-studied AFM system with fcc crystal structure and a 3Q noncollinear spin structure. Under exchange coupling with a magnet, a collinear A|B|A|B spin structure forms [39]. As a good spin filter, MgO is used to enhance MR and STT in FM-based junctions, where both the charge current and spin current are carried mainly by a small portion of the $k_{||}$ points in the two-dimensional Brillouin zone (2D BZ) [38,40]. The transport scheme in the AFM junctions has advantages over that in AFM|NM|AFM SVs [18], in which both the charge current and spin current are carried by almost all the $k_{||}$ points in the 2D BZ. In this calculation based on first principles, we predict large MR and STT in Fe|MgO|FeMn|Cu junctions. Specifically, MR ∼ 100% is predicted in a junction. Spin-dynamic simulations show that a current density of order 10^5 Acm^{-2} can switch a junction of 3-layered (3L) MgO.

This paper is organized as follows. In Sec. II, we provide our calculation details based on first-principle scattering theory. In Sec. III, we present our results on Fe|MgO|FeMn|Cu junctions with ordered and disordered crystal structures. Section IV presents our summary.

II. METHODS

In this work, we study the spin-dependent transport of the two terminal multilayers Fe|MgO|FeMn|Cu (see Fig. 1). Two magnetic structures with different spin structures (L-type and G-type) in the FeMn layer are considered. In detail, the L-type

*Corresponding author: jiaxingtao@hpu.edu.cn

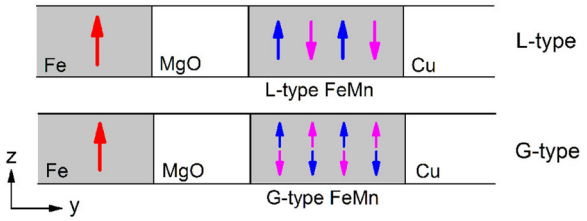

FIG. 1. Schematic two-terminal Fe|MgO|FeMn|Cu junction used in the calculations. Red arrow in the left lead indicates the fixed magnetization along the z axis; blue or pink arrow in FeMn indicates the sublattice magnetization $\mathbf{M_{1/2}}$. We define the antiferromagnetic order parameter as $\mathbf{l} = \mathbf{M}_1 - \mathbf{M}_2$, which is free in the x-z plane with relative angle θ with respective to the z axis.

is a higher symmetric A|B|A|B structure (upper panel of Fig. 1) in which the magnetization of layer A is compensated with that of layer B along the transport direction. The G-type is a lower symmetric structure (lower panel of Fig. 1) in which the magnetization of one sublattice is compensated both in-plane and out-of-plane with that of the another sublattice. The lateral supercell is used to match MgO with bcc-Fe and fcc-FeMn. The crystal MgO is reduced by 4% and rotated 45° to match the bcc-Fe. A 5 × 5 lateral supercell of Fe|MgO matches well with the 4 × 4 lateral supercell of fcc-FeMn (the mismatch is about 0.5%). A very small mismatch between the fcc-FeMn and fcc-Cu is neglected, and both FeMn and Cu are compressed along the epitaxial direction to maintain a volume equal to that of the bulk to match with Fe|MgO. The coherent potential approximation (CPA) is used for the potential of the FeMn alloys, and bulky potentials calculated self-consistently are put into a wave-function-matching (WFM) transport package [41]. During transport calculations, we consider the particle current along the (010) material growth direction, and a 40 × 40 k-mesh in the full 2D BZ is used to ensure good transport convergence. Two kinds of imperfects, spin flip (SF) in the site-ordered FeMn and oxygen vacancy (OV) at the interface close to MgO, are considered. Over 30 configurations are used in averaging the configuration convergence. More numerical details of the electronic structure and transport calculations can be found elsewhere [18,38,40].

III. RESULTS AND DISCUSSIONS

We next focus on the nonrelativistic structure-dependent MR, and then shift to STT in the antiferromagnetic region, and analyze the spin dynamics finally. Therein, two kinds of defects, OV and SF, are discussed.

A. Structure-dependent magnetoresistance

Figure 2 gives the MR in antiferromagnetic Fe|MgO|$Fe_{0.5}Mn_{0.5}$(16)|Cu junctions with clean interface as a function of MgO thickness; the numbers in the bracket indicate the thickness in atomic layers. We define $MR = [G(P) - G(AP)]/G(AP)$ with conductance $G = (e^2/h)/A \int Tr[t(k)t^{\circ}(k)]dk$ summarized in the 2D BZ at the Fermi level E_F. Here, P/AP denotes the parallel and/or antiparallel structure defined by the relative angle of $0/\pi$ between the magnetic order parameters of Fe and FeMn, t is the transmission part of the scattering

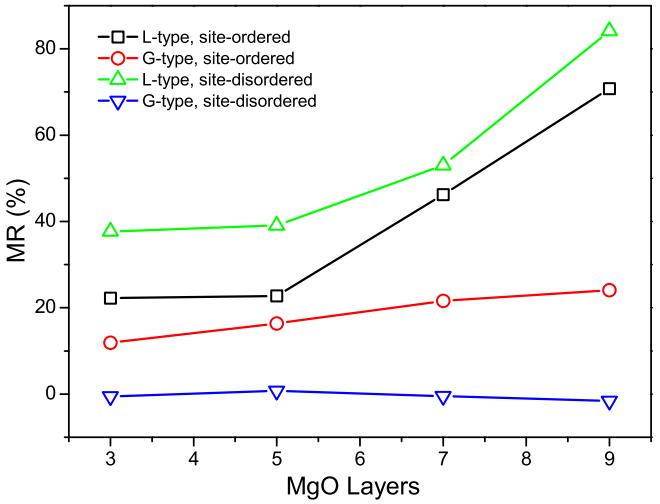

FIG. 2. Magnetoresistance as function of MgO thickness in the L-type and G-type antiferromagnetic Fe|MgO|$Fe_{0.5}Mn_{0.5}$(16)|Cu junctions with clean interface. The error bar is ∼5%.

matrix s, and A is the section area of the supercell. Both the site-ordered L-type and G-type junctions show notable MR, which is also sensitive to the thickness of MgO. The presence of the MR in the G-type junctions is related to the reduced symmetry, where only one Oxygen atom sitting directly on top of the Fe(Mn) atom of FeMn layer in one cell, and the change of antiferromagnetic order parameter would change the spin structure. Comparatively, we find zero MR (and negligible STT on the antiferromagnetic order parameter at relative angle of 90°) in a highly symmetric site-ordered G-type Fe|MgO(3)|bcc-$Fe_{0.5}Mn_{0.5}$(16)|bcc-Cu junction with one oxygen atom sitting directly on top of one up-spin Fe in the FeMn layer and another oxygen atom sitting on top of one down-spin Fe in one cell, where the reversal of the antiferromagnetic order parameter does not change the spin structure. When crystal sites are disordered, an enhanced MR is found in the L-type junctions, whereas a near-to-zero MR is obtained in the G-type junctions. With the exception of the site-disordered G-type junctions, MR increases as the barrier thickness increases. In detail, for site-ordered G-type junctions, MR increases from 12% in the 3L MgO case to 24% in the 9L MgO case. Comparatively, MR in the site-ordered L-type junctions increases quickly from 22% in the 3L MgO case to 71% in the 9L MgO case. If the crystal sites are disordered, an enhancement of 70%/20% is predicted in the L-type 3/9 L MgO junctions. Enhanced MR is also found in the L-type junctions with FeMn alloys of different

TABLE I. MR in site-disordered L-type Fe|MgO(n)|FeMn(16)|Cu junctions with clean interface at $\theta = 90°$.

n	3	5	7	9
$Fe_{0.25}Mn_{0.75}$	5	− 26	− 18	31
$Fe_{0.5}Mn_{0.5}$	35	39	53	84
$7Fe_{0.75}Mn_{0.25}$	10	101	135	100

concentrations (see Table I), where a MR ∼135% is found in a Fe|MgO(7)|$Fe_{0.75}Mn_{0.25}$(16)|Cu junction.

Similar to the well-studied MgO-based junctions, MR in the antiferromagnetic Fe|MgO|FeMn|Cu junctions is sensitive to OV. For the L-type junctions (including both site-ordered and site-disordered) and the site-disordered G-type junctions, about 10% OV at the interfaces near to MgO degrade the MR in Fe|MgO(3)|$Fe_{0.5}Mn_{0.5}$(16)|Cu by one order of magnitude compared with clean junctions (several ten percent for clean junctions to several percent for dirty junctions; see Table II). For thicker MgO junctions, we get similar results. Hence, to achieve larger MR, the junctions should be as clean as possible.

Spin disorder, such as SF, changes the magnetization and shows up in effects on spin-dependent transport. In Table II, we list MR in Fe|MgO(3)|$Fe_{0.5}Mn_{0.5}$(16)|Cu with 10% SFs in FeMn alloy. The SF shows less effect on the MR in the L-type junctions than in the G-type junctions. For thicker MgO junctions, we obtain similar results.

B. Spin transfer torques

In driving the magnetic order parameter [42,43], STT is the favored means as they can be induced by a bias voltage and thermal gradient [38,44]. With small bias voltages, STT is almost linear with bias voltage, especially in the MTJs [45], for which "torkance" (τ) can be introduced. The magnetic structure of an AFM can be described by the sublattice magnetizations $\mathbf{M}_j$ ($j = 1,2$ for the simplest case) with total magnetization $\mathbf{m} = \mathbf{M}_1 + \mathbf{M}_2$ and antiferromagnetic order parameter $\mathbf{l} = \mathbf{M}_1 - \mathbf{M}_2$. Indeed, STT can also be used to drive the antiferromagnetic order parameter [17–27]. We denote the STT acting on the total magnetization $\mathbf{m}$ and antiferromagnetic order parameter $\mathbf{l}$ as τ_m ($\tau_m = \tau_{m_1} + \tau_{m_2}$) and τ_l ($\tau_l = \tau_{m_1} - \tau_{m_2}$), respectively. First, let us take a look at a simple model with a thin antiferromagnetic layer interacting with a spin current. For one sublattice magnetization $\mathbf{M}_j$ in AFM, the STT applied to $\mathbf{M}_j$ is proportional to $\mathbf{M}_j \times \mathbf{M}' \times \mathbf{M}_j$ (in-plane) and $\mathbf{M}_j \times \mathbf{M}'$(out-of-plane) with $\mathbf{M}'$ the spin current source. For the simplest AFM, the in-plane/out-of-plane STT on $\mathbf{M}_{1(2)}$ follows the same/opposite direction as that on $\mathbf{M}_{2(1)}$. Hence, the out-of-plane component of τ_l ($\tau_l^{\perp}$) and the in-plane component of τ_m ($\tau_m^{||}$) would be enhanced, whereas the in-plane component of τ_l ($\tau_l^{||}$) and the out-of-plane component of τ_m ($\tau_m^{\perp}$) would vanish. The model analysis is suitable for a classical system but is invalid [19] in structures with quantum states dominating. In classical cases, for which $\tau_l/\tau_m \to 0$, the spin dynamics are dominated by τ_m with ultrahigh working frequencies [20–27]. The spin-glass state can be considered as classical. A large deviation from the model analysis is observed in the Fe|MgO|FeMn|Cu junction, as shown in below, where the spin transport is dominated by quantum states.

From the dependence of STT on MgO thickness [Fig. 3(a)] for both the site-ordered and site-disordered Fe|MgO|$Fe_{0.5}Mn_{0.5}$|Cu junctions with clean interface at relative angle of 90°, we find that: (1) both τ_l and τ_m exponentially decrease as the MgO thickness is larger than 3 L. The enhanced STT from the interfacial resonance states in the ultra-thin (3L) barrier appears responsible for this deviation. The marked τ_l (at relative angle of 90°) in the site-ordered G-type junction is related to the reduced symmetry in the lateral supercell structure,

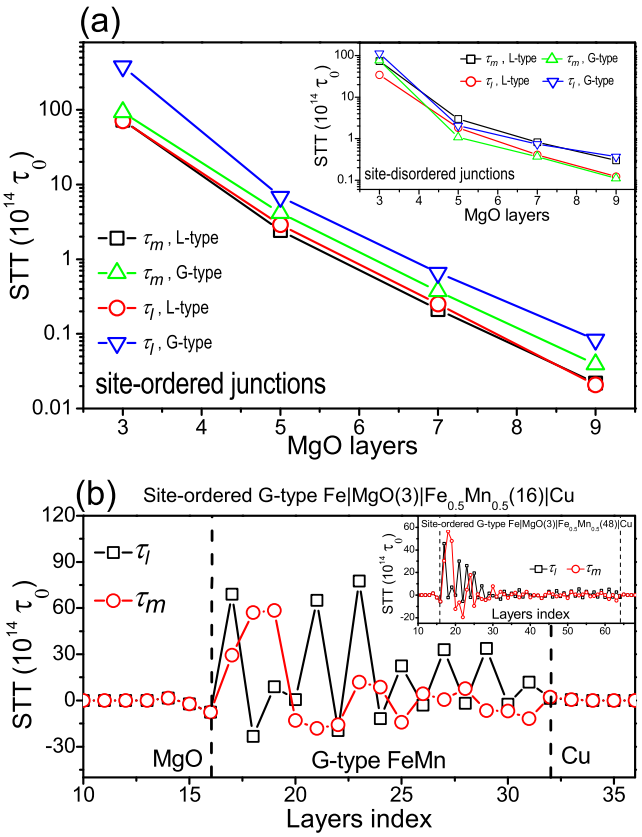

FIG. 3. Spin transfer torque as a function of MgO thickness (a) in site-ordered antiferromagnetic Fe|MgO|$Fe_{0.5}Mn_{0.5}$(16)|Cu junctions with clean interface at relative angle of 90° (Inset: similarly for site-disordered Fe|MgO(3)|$Fe_{0.5}Mn_{0.5}$(16)|Cu junctions with clean interface). (b) Layer-dependent spin transfer torque in site-ordered G-type Fe|MgO(3)|$Fe_{0.5}Mn_{0.5}$(16)|Cu junctions at relative angle of 90° (Inset: similarly for site-disordered G-type Fe|MgO(3)|$Fe_{0.5}Mn_{0.5}$(48)|Cu junctions).

as discussed in the above section, which follows a simple sine relation with respect to the relative angle rather than a sin(2θ) relation [19] presented in a simple FM|NM|AFM model. (2) τ_l is comparable to τ_m for both site-ordered and site-disordered junctions of L-type and G-type. Consequently, the dynamics of the antiferromagnetic-order parameter would be driven by τ_l rather than τ_m [17,28], with working frequency $\omega_A = \gamma H_A$ controlled by the anisotropic effective field H_A. Note that ω_A is considerably lower than that for the τ_m-driven case $\omega = \sqrt{2\omega_A\omega_E}$ with $\omega_E = \gamma H_E$ and H_E is the exchange field. In detail, τ_l in the site-ordered and site-disordered L/G-type Fe|MgO(3)|$Fe_{0.5}Mn_{0.5}$(16)|Cu junctions are $71/382 \times 10^{14}\tau_0$ ($\tau_0 \equiv \frac{\hbar}{2e}k\Omega^{-1}m^{-2}$) and $22/122 \times 10^{14}\tau_0$, respectively; see list in Table II. Specifically, τ_l in the G-type junctions is several times larger than that in the L-type junctions, and is sensitive to site disorder. In comparison, $\tau_m^{||}$ is not only stable to site disorder but also to spin configurations, as demonstrated in Table II. Furthermore, $\tau_m^{||}$ calculated by the WFM method is consistent well with that estimated from transmissions via a free-electron model [46].

Moreover, τ_l is strongly dependent on the thickness of FeMn, whereas τ_m is almost constant. The behavior of τ_l (as a

TABLE II. In-plane spin transfer torque in site-ordered and site-disordered L-/G-type Fe|MgO(n)| $Fe_{0.5}Mn_{0.5}$(16)|Cu junctions with clean interface with $\theta = 90^\circ$. The resistance area $RA = 1/G(E_F)$. η_m and η_l are the spin transfer efficiency of STT on the total magnetization **m** and antiferromagnetic order parameter **l**, respectively. V_C and J_C are the critical bias voltage and critical current density to switch the antiferromagnetic order parameter, circularly. We assess V_C and J_C by choosing easy uniaxial anisotropy field of 20 mT and Gilbert damping coefficient of 0.01 in the spin dynamics simulations.

n (L)	MR (%)	RA ($\Omega\mu m^2$)	τ_m (τ_0)	τ_l (τ_0)	η_m ($\hbar/2e$)	η_l ($\hbar/2e$)	V_C (mV)	J_C (10^5 Acm^{-2})
Site-ordered cases								
3	22/12	0.11/0.093	73/93	71/381	0.75/0.80	0.74/3.3	0.17/0.03	1.5/0.35
5	23/16	3.6/2.2	2.4/4.2	2.9/3.9	0.80/0.85	0.96/0.79	4.2/3.2	1.2/1.4
7	46/22	39/26	0.21/0.37	0.25/0.56	0.76/0.88	0.89/1.3	49/22	1.3/0.86
9	71/24	352/245	0.02/0.04	0.02/0.08	0.72/0.89	0.68/1.9	593/147	1.7/0.60
3[a]	4/2	0.036/0.034	92/97	74/20	0.31/0.30	0.25/0.061	0.17/0.63	4.5/19
3[b]	22/3	0.11/0.098	80/94	20/4	0.81/0.85	0.20//0.034	0.62/3.3	5.7/34
Site-disordered cases								
3	35/0.56	0.13/0.11	72/76	22/6.3	0.83/0.77	0.25//0.064	0.56/2.0	4.5/18
5	39/0.71	3.7/2.3	0.92/1.07	0.91/0.13	0.31/0.23	0.31/0.028	13.5/93	3.7/41
7	53/−0.49	34/27	0.31/0.36	0.21/0.23	0.99/0.83	0.65/0.54	60/53	1.7/2.1
9	84/−1.59	313//239	0.035/0.04	0.14/0.18	0.98/0.91	3.8/4.1	89/66	0.30/0.29
3[1]	4/3	0.039/0.042	88/74	35/33	0.32/0.29	0.13/0.13	0.35/0.36	8.9/8.8
3[2]	27/5.7	0.12/0.12	75/75	37/20	0.81/0.75	0.39/0.20	0.34/0.61	2.9/5.6

[a]10% OV at interfaces close to MgO.
[b]10% SF in $Fe_{0.5}Mn_{0.5}$.

function of FeMn thickness) is different from the recent model calculations [17,28], where a AFM|NM|AFM spin valve was studied with the spin torque acting on the antiferromagnetic order parameter increasing linearly with the thickness of AFM layers. The difference seems to be the combination effect of an interfacial effect (as shown in Fig. 3) and multiple scattering (as shown in Fig. 4).

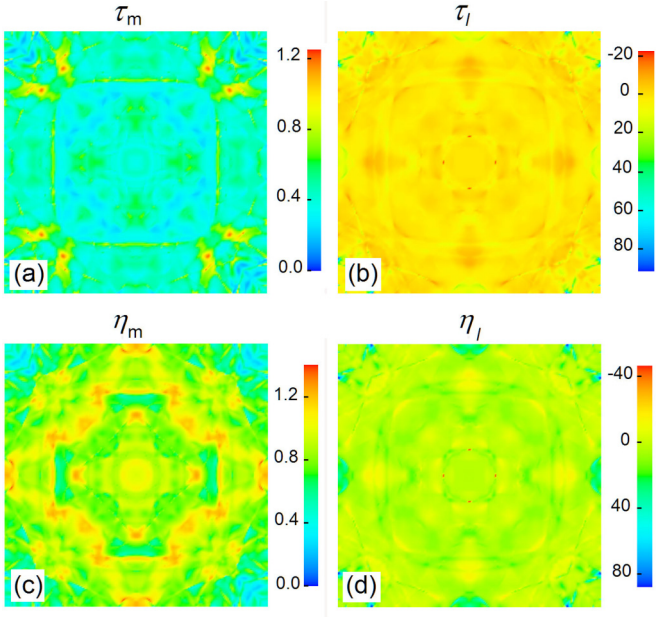

FIG. 4. (a, b) $k_{||}$ resolved STT and (c, d) spin transfer efficiency $\eta = \tau(k)/G(k)$ in units of $\hbar/2e$ with $G(k) = (e^2/h)Tr[t(k)t^\dagger(k)]$ in site-ordered G-type Fe|MgO(3)|$Fe_{0.5}Mn_{0.5}$(16)|Cu junction with clean interface at relative angle of 90°.

To check the spin-transfer behavior in the antiferromagnetic FeMn, we present the layer-dependent spin torque in the site-ordered G-type Fe|MgO(3)|$Fe_{0.5}Mn_{0.5}$(16)|Cu junctions with clean interface in Fig. 3(b). Here, both τ_l and τ_m decrease quickly with distance from the MgO|FeMn interface [the behavior is more clear for thicker FeMn layers; see inset of Fig. 3(b)], indicating that the spin torque may be an interfacial effect. The behavior is very similar to spin transfer in FMs. In comparison, the spin torque in an antiferromagnetic metal-based spin valve spans the whole antiferromagnetic region [17,18,28].

Of equal importance as the magnitude of spin torque is the spin transfer efficiency in assessing the spin transfer process. We give the spin transfer efficiency in Table II for both STTs as applied to total magnetization and antiferromagnetic order parameter. The spin transfer efficiency of the STT on the total magnetization (η_m) is seen to be close to but less than one unit for most cases, which is quite stable in the presence of defects such as OV and SF. The high-spin transfer efficiency is related to strong spin filtering of the MgO barrier. However, the spin transfer efficiency of the STT for the antiferromagnetic order parameter (η_l) is sensitive to not only barrier thickness but also defects (Table II). Surprisingly, we find η_l is larger than one unit in several junctions. For example, η_l of 3.3 $\hbar/2e$ is observed in the site-ordered G-type Fe|MgO(3)|$Fe_{0.5}Mn_{0.5}$(16)|Cu junction with clean interface at the relative angle of 90°. By comparing the STT with η in the junctions, we find that high η contributes largely in enhancing STT.

To check the enhanced τ_l and η_l, we give $k_{||}$-resolved τ and η in the site-ordered G-type Fe|MgO(3)|$Fe_{0.5}Mn_{0.5}$(16)|Cu junction with clean interface at relative angle of 90° (Fig. 4). Both τ_m and τ_l are mainly from hot spots in the 2D BZ, and the pattern of the former is close to that of the transmission,

indicating that spin transfer is carried mainly by resonance states. Hot $k_{||}$ points with maximum $\eta_m \sim 1.4\hbar/2e$ and $\eta_l \sim 85\hbar/2e$ are observed, indicating that spin transfer occurs more than once. Considering the relative angle of 90° between the magnetization of the left lead and the order parameter of FeMn, the spin transfer efficiency contributed by the MgO|FeMn interface does not exceed one unit, and multiple spin transfer may stem from the FeMn region.

Replacing Mn by Fe, a Fe|MgO|AFM-Fe|Cu junction is formed. We find τ_l in both the L-type and G-type junctions are several times larger than τ_m. In detail, $\tau_m \sim 146/81 \times 10^{14}\tau_0$ and $\tau_l \sim 486/346 \times 10^{14}\tau_0$ are observed in the L-/G-type Fe|MgO(3)|AFM-Fe(16)|Cu junctions at relative angle of 90°. That is, multiple spin transfer is found in both the L-type and G-type junctions.

Furthermore, OV shows less effect on τ_m for both site-ordered and site-disordered junctions. τ_m of $97/92 \times 10^{14}\tau_0$ and $88/74 \times 10^{14}\tau_0$ are found in the site-ordered and site-disordered G − /L − type Fe|MgO(3)|$Fe_{0.5}Mn_{0.5}$(16)|Cu junctions with 10% OV at Fe|MgO and FeMn|MgO interfaces, respectively; see Table II. They are slightly larger than those in the correspondingly clean junctions, respectively. The enhancement in spin-dependent transmissions from vertex scattering in the dirty junctions may be responsible for the enhanced spin torque. In comparison, OV at interfaces would enhance τ_l in the G-type junctions but suppress τ_l in the L-type junctions.

Similar to OV, τ_l/τ_m is sensitive/insensitive to SF in the antiferromagnetic region. τ_m of $80/94 \times 10^{14}\tau_0$, and $75/75 \times 10^{14}\tau_0$ and τ_l of $20/4 \times 10^{14}\tau_0$ and $37/20 \times 10^{14}\tau_0$ are found in the site-ordered and site-disordered L-/G-type Fe|MgO(3)|$Fe_{0.5}Mn_{0.5}$(16)|Cu junction in the presence of 10% SF, respectively. Hence, to achieve large τ_l, spin disorder should be avoided.

From angular-dependent STT, we can estimate the critical switching bias voltage and current by a phenomenological Landau-Lifshitz-Gilbert (LLG) equation [17]. We find that the angular dependency in STT for both L-type and G-type junctions follows simple trigonometric functions. Considering a single AFM domain with easy uniaxial anisotropic field $H_K \sim 20$ mT along the z direction and Gilbert damping coefficient of 0.01, we estimated the critical switching bias voltage V_C and critical current density J_C in Fe|MgO|$Fe_{0.5}Mn_{0.5}$(16)|Cu junctions (Table II). As barrier thickness increases, V_C increases exponentially. Also $G(E_F)$ ($G = 1/RA$) decreases exponentially, while J_C, the product of V_C and $G(E_F)$, is of order 10^5 Acm^{-2} and changes less with MgO thickness. For example, V_C of 0.17/0.032 mV and J_C of $1.5/0.35 \times 10^5$ Acm^{-2} is found in site-ordered L-/G-type Fe|MgO(3)|$Fe_{0.5}Mn_{0.5}$(16)|Cu junctions. Both V_C and J_C are about one order smaller than those in Fe|MgO|Fe junctions [38,47] with the same barrier thickness, respectively. The reduction in V_C and J_C, compared with those in Fe|MgO|Fe junctions, should be related with: (1) enhanced spin torque by multiple spin transfers in the AFM region (Fig. 4), (2) absence of shape anisotropy, and (3) symmetric angular dependence in spin torque. Furthermore, the uniaxial anisotropy in AFM depends on thickness. This is similar to that in FM. A small H_K of less than 1 mT in thin FeMn has been estimated in the NiFe|FeMn|CoFe multilayer [48]. Using this parameter value, V_C and J_C would be one order smaller than the numbers above.

So far, we conclude that the spin dynamics in the antiferromagnetic Fe|MgO|FeMn|Cu junctions is driven by τ_l with low working frequency. The conclusion is weakly contingent on the right lead materials, and similar spin dynamic behaviors are observed in junctions with the right Cu lead replaced by metals such as bcc-Cr, fcc-Ag, and fcc-pt. Moreover, the spin dynamics in an AFM driven by τ_m is as effective as that driven by τ_l. For example, the spin Hall effect [49,50] at the NM|AFM interface can induce pure τ_m in the absence of a particle current across the AFM, which driving the spin dynamics at very high working frequency.

However, it is hard to observe MR in FeMn-based structures experimentally, partly because the spin structure is complex [51–54] in FeMn. If the spin structure in FeMn is simply collinear, MR would be easily observed experimentally. An experimental study [39] shows that the introduction of an exchange bias in the FeMn|Co interface can collinearly stabilize the antiferromagnetic order parameter. Moreover, the collinear spin structure is also experimentally demonstrated in bulky antiferromagnetic Mn_2Au [55] and CuMnAs [56]. We expect an experimentally observed nonrelativistic MR in this collinear antiferromagnetic spin structure.

IV. SUMMARY

Based on first-principles scattering theory, we predict large MR and STT in antiferromagnetic Fe|MgO|FeMn|Cu junctions. A larger MR ∼ 100% was found in one junction. Spin torque acting on antiferromagnetic order parameters τ_l is the same order as that acting on the total magnetization τ_m. The marked MR and τ_l in the site-ordered G-type junctions are related to reduced symmetry in the system. Both MR and STT are sensitive to interfacial OV and SF in the FeMn region. Spin dynamics, studied using a phenomenological LLG equation, suggest that τ_l rather than τ_m drives the magnetic dynamics. An electronic bias of order 10^{-1} mV and current density of order 10^5 Acm^{-2} are predicted to efficiently switch a junction with a 3L MgO barrier, which are one order smaller than those in the Fe|MgO|Fe junction with the same barrier thickness, respectively. Multiple spin transfer existing in the antiferromagnetic region may be responsible for the enhanced spin torque and small switching current density.

ACKNOWLEDGMENTS

X.J. thanks Ke Xia at BNU for the suggestion of the calculations. We gratefully acknowledge financial support from National Natural Science Foundation of China under Grants No. 11274094 and No. 51332007. X.J. also acknowledges financial support from HPU (Grants No. B2012-021 and No. T2016-2).

X. Jia and H. Tang contributed equally to this study and share first authorship.

[1] A. MacDonald and M. Tsoi, Philos. Trans. R. Soc. London A **369**, 3098 (2011).
[2] T. Jungwirth, X. Marti, P. Wadley, and J. Wunderlich, Nat. Nanotech. **11**, 231 (2016).
[3] X. Mart, I. Fina, and T. Jungwirth, IEEE T. MAGN. **51**, 1 (2015).
[4] A. Kimel, A. Kirilyuk, A. Tsvetkov, R. Pisarev, and T. Rasing, Nature **429**, 850 (2004).
[5] A. Kimel, A. Kirilyuk, P. Usachev, R. Pisarev, A. Balbashov, and T. Rasing, Nature **435**, 655 (2005).
[6] T. Satoh, S.-J. Cho, R. Iida, T. Shimura, K. Kuroda, H. Ueda, Y. Ueda, B. A. Ivanov, F. Nori, and M. Fiebig, Phys. Rev. Lett. **105**, 077402 (2010).
[7] S. Wienholdt, D. Hinzke, and U. Nowak, Phys. Rev. Lett. **108**, 247207 (2012).
[8] X. Marti, I. Fina, C. Frontera, J. Liu, P. Wadley, Q. He, R. Paull, J. Clarkson, J. Kudrnovský, I. Turek *et al.*, Nat. Mater. **13**, 367 (2014).
[9] Y. Y. Wang, C. Song, B. Cui, G. Y. Wang, F. Zeng, and F. Pan, Phys. Rev. Lett. **109**, 137201 (2012).
[10] C. Wang, H. Seinige, G. Cao, J.-S. Zhou, J. B. Goodenough, and M. Tsoi, Phys. Rev. X **4**, 041034 (2014).
[11] I. Fina, X. Marti, D. Yi, J. Liu, J. Chu, C. Rayan-Serrao, S. Suresha, A. Shick, J. Železný, T. Jungwirth *et al.*, Nat. Commun. **5**, 4671 (2014).
[12] B. Park, J. Wunderlich, X. Marti, V. Holý, Y. Kurosaki, M. Yamada, H. Yamamoto, A. Nishide, J. Hayakawa, H. Takahashi *et al.*, Nat. Mater. **10**, 347 (2011).
[13] W. Zhang, M. B. Jungfleisch, W. Jiang, J. E. Pearson, A. Hoffmann, F. Freimuth, and Y. Mokrousov, Phys. Rev. Lett. **113**, 196602 (2014).
[14] T. Shang, H. L. Yang, Q. F. Zhan, Z. H. Zuo, Y. L. Xie, L. P. Liu, S. L. Zhang, Y. Zhang, H. H. Li, and B. M. Wang, J. Appl. Phys. **120**, 133901 (2016).
[15] L. Frangou, S. Oyarzún, S. Auffret, L. Vila, S. Gambarelli, and V. Baltz, Phys. Rev. Lett. **116**, 077203 (2016).
[16] S. Loth, S. Baumann, C. P. Lutz, D. Eigler, and A. J. Heinrich, Science **335**, 196 (2012).
[17] A. S. Núñez, R. A. Duine, P. Haney, and A. H. MacDonald, Phys. Rev. B **73**, 214426 (2006).
[18] Y. Xu, S. Wang, and K. Xia, Phys. Rev. Lett. **100**, 226602 (2008).
[19] P. M. Haney and A. H. MacDonald, Phys. Rev. Lett. **100**, 196801 (2008).
[20] H. Gomonay and V. Loktev, J. Magn. Soc. Jpn. **32**, 535 (2008).
[21] H. V. Gomonay and V. M. Loktev, Phys. Rev. B **81**, 144427 (2010).
[22] A. C. Swaving and R. A. Duine, Phys. Rev. B **83**, 054428 (2011).
[23] E. G. Tveten, A. Qaiumzadeh, O. A. Tretiakov, and A. Brataas, Phys. Rev. Lett. **110**, 127208 (2013).
[24] R. Cheng, J. Xiao, Q. Niu, and A. Brataas, Phys. Rev. Lett. **113**, 057601 (2014).
[25] R. Cheng, M. W. Daniels, J.-G. Zhu, and D. Xiao, Phys. Rev. B **91**, 064423 (2015).
[26] K. M. D. Hals, Y. Tserkovnyak, and A. Brataas, Phys. Rev. Lett. **106**, 107206 (2011).
[27] R. Cheng and Q. Niu, Phys. Rev. B **89**, 081105 (2014).
[28] Hamed Ben Mohamed Saidaoui, A. Manchon, and X. Waintal, Phys. Rev. B **89**, 174430 (2014).
[29] F. A. Perez, P. Borisov, T. A. Johnson, T. D. Stanescu, R. Trappen, M. B. Holcomb, D. Lederman, M. R. Fitzsimmons, A. A. Aczel, and T. Hong, Phys. Rev. Lett. **114**, 097201 (2015).
[30] E. G. Tveten, A. Qaiumzadeh, and A. Brataas, Phys. Rev. Lett. **112**, 147204 (2014).
[31] A. Manchon and S. Zhang, Phys. Rev. B **79**, 094422 (2009).
[32] A. Brataas and K. M. Hals, Nat. Nanotech. **9**, 86 (2014).
[33] F. Freimuth, S. Blügel, and Y. Mokrousov, Phys. Rev. B **92**, 064415 (2015).
[34] O. Gomonay, T. Jungwirth, and J. Sinova, Phys. Rev. Lett. **117**, 017202 (2016).
[35] W. Zhang, M. B. Jungfleisch, F. Freimuth, W. Jiang, J. Sklenar, J. E. Pearson, J. B. Ketterson, Y. Mokrousov, and A. Hoffmann, Phys. Rev. B **92**, 144405 (2015).
[36] V. Tshitoyan, C. Ciccarelli, A. P. Mihai, M. Ali, A. C. Irvine, T. A. Moore, T. Jungwirth, and A. J. Ferguson, Phys. Rev. B **92**, 214406 (2015).
[37] J. Linder, Phys. Rev. B **84**, 094404 (2011).
[38] X. Jia, K. Xia, and G. E. W. Bauer, Phys. Rev. Lett. **107**, 176603 (2011).
[39] W. J. Antel, F. Perjeru, and G. R. Harp, Phys. Rev. Lett. **83**, 1439 (1999).
[40] Y. Ke, K. Xia, and H. Guo, Phys. Rev. Lett. **105**, 236801 (2010).
[41] S. Wang, Y. Xu, and K. Xia, Phys. Rev. B **77**, 184430 (2008).
[42] J. C. Slonczewski, J. Magn. Magn. Mater. **159**, L1 (1996).
[43] L. Berger, Phys. Rev. B **54**, 9353 (1996).
[44] G. E. Bauer, E. Saitoh, and B. J. van Wees, Nat. Mater. **11**, 391 (2012).
[45] X. Jia, K. Xia, Y. Ke, and H. Guo, Phys. Rev. B **84**, 014401 (2011).
[46] J. Slonczewski, J. Magn. Magn. Mater. **247**, 324 (2002).
[47] P. Ogrodnik, G. E. W. Bauer, and K. Xia, Phys. Rev. B **88**, 024406 (2013).
[48] H.-C. Choi, C.-Y. You, K.-Y. Kim, J.-S. Lee, J.-H. Shim, and D.-H. Kim, Phys. Rev. B **81**, 224410 (2010).
[49] Y.-T. Chen, S. Takahashi, H. Nakayama, M. Althammer, S. T. B. Goennenwein, E. Saitoh, and G. E. W. Bauer, Phys. Rev. B **87**, 144411 (2013).
[50] H. Nakayama, M. Althammer, Y.-T. Chen, K. Uchida, Y. Kajiwara, D. Kikuchi, T. Ohtani, S. Geprägs, M. Opel, S. Takahashi *et al.*, Phys. Rev. Lett. **110**, 206601 (2013).
[51] D. Spišák and J. Hafner, Phys. Rev. B **61**, 11569 (2000).
[52] K. Nakamura, T. Ito, A. J. Freeman, L. Zhong, and J. Fernandez-de Castro, Phys. Rev. B **67**, 014405 (2003).
[53] M. Ekholm and I. A. Abrikosov, Phys. Rev. B **84**, 104423 (2011).
[54] W. Kuch, L. I. Chelaru, F. Offi, J. Wang, M. Kotsugi, and J. Kirschner, Phys. Rev. Lett. **92**, 017201 (2004).
[55] V. M. T. S. Barthem, C. Colin, H. Mayaffre, M.-H. Julien, and D. Givord, Nat. Commun. **4**, 2892 (2013).
[56] P. Wadley, V. Novák, R. Campion, C. Rinaldi, X. Marti, H. Reichlová, J. Železný, J. Gazquez, M. Roldan, M. Varela *et al.*, Nat. Commun. **4**, 2322 (2013).